J. Indones. Math. Soc. (MIHMI)
Vol. 11, No. 2 (2005), pp. 101–119.

# MODELING OF QUASI-GUIDING LIGHT WITHIN THE LOWER REFRACTIVE INDEX CORE LAYER(S)

H.P. Uranus, H.J.W.M. Hoekstra, and E. van Groesen

**Abstract.** It is well known that light can be guided within layer(s) having refractive index higher than that of the surroundings by means of the total internal reflection principles. However, using a proper structure, light can also be quasi-confined into layer(s) with refractive indices lower than the surroundings. In this case the light is quasi-guided. In this work, we will show that using proper mathematical tools, we can model the latter case of confining light. We used the Galerkin finite element method with Sommerfeld-like boundary conditions to conduct numerical investigations on this class of structures. We investigate numerically the properties of the anti-resonant reflecting optical waveguides (ARROW), leaky step- and graded-index waveguides, planar Bragg and hollow waveguides. Through the modal solutions (i.e. the complex-valued mode indices and modal field profiles), we present an intuitive interpretation of the unique properties of such structures, e.g. the anti-crossing between core and cladding resonance modes in ARROW, the growing-up of field in the high-index substrate/cladding of leaky waveguides, and the relation between Bragg and hollow waveguides.

## 1. INTRODUCTION

Nowadays, a lot of daily activities take benefits from the availability of high-speed tele- or data-communication networks. The backbones of these networks are optical fibers as the transmission line which provide the huge bandwidth required to carry all the information between tele- or data-communication centers; which may be located within just the same building or separated in different continents. It is

Received 28 June 2004, Revised 4 February 2005, Accepted 8 February 2005.
*2000 Mathematics Subject Classification*: 78A50, 78M10, 65Z05, 65N45.
*Key words and Phrases*: leaky modes, finite element method, boundary conditions, ARROW, Bragg waveguide, hollow waveguide.

well known that light can be guided within optical fibers due to the presence of the higher refractive index of the core and the lower refractive index of the surrounding cladding. The mechanism of this light confinement can be intuitively explained by means of Snell's law, which leads to the so-called total internal reflection principles for this composition of refractive indices.

However, using proper structures, light can also be quasi-confined into the media with refractive indices lower than that of the surrounding. In this case, the light is quasi-guided and the modes are known as the leaky modes. This kind of phenomenon have been modeled using various method; like the perturbation method [10], the transfer matrix method [4], the transverse resonance method [2], the finite difference method (FDM) [3], the beam propagation method (BPM) [9], etc. However, there are still many interesting aspects of such structures, which have not been reported yet. In this work, we will show that using proper mathematical tools, in our case is numerical method with proper boundary conditions, we can model this phenomenon. We used the Galerkin finite element method (FEM) with Sommerfeld-like boundary conditions to conduct numerical investigations on this class of structures. We numerically investigate the properties of various leaky structures, like the anti-resonant reflecting optical waveguides (ARROW), leaky step- and graded-index waveguides, Bragg and hollow waveguides. Through the modal solutions (i.e. the complex-valued mode indices and modal field profiles), we present an intuitive interpretation of the unique properties of such structures, e.g. the anti-crossing between core and cladding resonance modes in ARROW, the growing-up of field in the high-index substrate/cladding of leaky waveguides, and the relation between Bragg and hollow waveguides. To simplify the problem, we have restricted ourselves to analyze planar structures composed of non-magnetic materials with dielectric anisotropy of diagonal permittivity tensors.

## 2. FINITE ELEMENT FORMULATION FOR LEAKY STRUCTURES

For the materials considered in this work, where the principal axes of the anisotropy are assumed to be parallel with the Cartesian coordinate system of the waveguide, the permittivity tensor can be expressed in a diagonal form as

$$\overline{\overline{\varepsilon}} = \varepsilon_0 \begin{bmatrix} n_{xx}^2 & 0 & 0 \\ 0 & n_{yy}^2 & 0 \\ 0 & 0 & n_{zz}^2 \end{bmatrix}$$

with $\varepsilon_0$ denoting the free space permittivity, while $n_{xx}$, $n_{yy}$, and $n_{zz}$ are refractive indices associated with the $x$, $y$, and $z$ components of the electric field, respectively. By assuming that the waveguide is composed of non-magnetic and source-free material, and that the refractive indices change only in the $x$ direction, while the $z$-axis is the propagation direction, we can get from Maxwell's equations, the uncoupled

wave equations that govern the propagation of light within the structure as follows

$$\left[\partial_{xx} + k_0^2\left(n_{yy}^2(x) - n_{eff}^2\right)\right] E_y(x) = 0 \tag{1}$$

for transverse electric (TE), and

$$\left[\partial_x\left(\frac{1}{n_{zz}^2(x)}\partial_x\right) + k_0^2\left(1 - \frac{n_{eff}^2}{n_{xx}^2(x)}\right)\right] H_y(x) = 0 \tag{2}$$

for transverse magnetic (TM) polarization. In eqs. (1) and (2); $k_0$, $n_{eff}$, $E_y$, and $H_y$ denote the free space wavenumber, mode effective index, electric and magnetic fields parallel to the $y$-axis, respectively. To investigate the phenomenon of quasi-guiding light within the lower refractive index core layer(s), we numerically solve eq. (1) for TE or (2) for TM with boundary conditions that allow outgoing radiation toward the high index exterior domain and evanescent decay toward the low index exterior domain.

The Galerkin FEM scheme being used for this work has been presented in our previous work [11], but for convenience it will be briefly repeated here. Following the Galerkin procedure, performing partial integration of terms that contain second order derivatives, discretizing the computational domain, and using of the continuity of $E_y$, $H_y$, $\partial_x E_y$, and $(1/n_{zz}^2)\partial_x H_y$ across material interfaces, the discretized weak formulation of the corresponding equations can be written as

$$w\partial_x\varphi|_{\partial\Omega} + \sum_{e=1}^{N}\int_{\Omega_e}\left[-\left(\partial_x w\right)\left(\partial_x\varphi\right) + k_0^2\left(n_{yy}^2 - n_{eff}^2\right)w\varphi\right]dx = 0 \tag{3}$$

for TE and

$$\frac{1}{n_{zz}^2}w\partial_x\varphi\Big|_{\partial\Omega} + \sum_{e=1}^{N}\int_{\Omega_e}\left[-\frac{1}{n_{zz}^2}\left(\partial_x w\right)\left(\partial_x\varphi\right) + k_0^2\left(1 - \frac{n_{eff}^2}{n_{xx}^2}\right)w\varphi\right]dx = 0 \tag{4}$$

for TM polarization, with $w$, $\partial\Omega$, $\Omega_e$, and $N$ denote the weight function, the computational boundary, the elements, and the number of elements; respectively. For notational simplicity, $\varphi$ has been used to denote both $E_y$ in eq. (3) and $H_y$ in eq. (4). Approximating the function $\varphi$ within each element by extrapolation of first-order-polynomial basis functions, using the same basis functions as the weight functions, and evaluating the integral analytically, we can then express eqs. (3) and (4) in matrix generalized eigenvalue equations as follows:

$$\mathbf{C}^{TE}\{\boldsymbol{\varphi}\} + \left(\mathbf{A}^{TE} - n_{eff}^2\mathbf{B}^{TE}\right)\{\boldsymbol{\varphi}\} = \{\mathbf{0}\} \tag{5}$$

and

$$\mathbf{C}^{TM}\{\boldsymbol{\varphi}\} + \left(\mathbf{A}^{TM} - n_{eff}^2\mathbf{B}^{TM}\right)\{\boldsymbol{\varphi}\} = \{\mathbf{0}\} \tag{6}$$

respectively, where $\mathbf{A}^{TE}$, $\mathbf{B}^{TE}$, $\mathbf{A}^{TM}$, and $\mathbf{B}^{TM}$ are sparse tridiagonal matrices that result from the evaluation of the corresponding integral terms within eqs. (3) and (4), while $\mathbf{C}^{TE}$ and $\mathbf{C}^{TM}$ are matrices associated with the boundary terms. Here,

$$\{\boldsymbol{\varphi}\} = [\varphi_1 ... \varphi_{N+1}]^T$$

where the subscript denotes the node number, are column vectors representing the discretized electric field for eq. (5) and magnetic field for eq. (6) at nodal points.

To evaluate the boundary terms in eqs. (3) and (4), we impose Sommerfeld-like boundary conditions as follows. At boundary where the refractive index ($n_{yy}$ for TE or $n_{xx}$ for TM, see explanation below) of the exterior domain is higher than the mode index, the wave is expected to leak out toward the exterior domain. Hence, by assuming *exp(i$\omega$t)* time dependence, Sommerfeld radiation boundary conditions

$$(\partial_r + ik_r)\,\varphi\,(r) = 0 \tag{7}$$

can be used. In eq. (7) $r$ and $k_r$ denote the transverse direction and the transverse wavenumber, respectively. At boundary where the refractive index is lower than the mode index, the field is expected to evanescently decay in transversal direction into the exterior domain, hence radiation boundary conditions is no more suitable for this purpose. However, we still can use eq. (7) for this purpose if we choose $k_r$ as a complex quantity. The solution of eq. (7) clearly shows that the field will radiate out if we have Re($k_r$)>0 and decay if Im($k_r$)<0. Solving the wave equations for the (assumed) homogeneous exterior domain will lead to $k_r = k_0\sqrt{n_{yy}^2 - n_{eff}^2}\Big|_{\partial\Omega}$ for TE and $k_r = k_0 \frac{n_{zz}}{n_{xx}}\sqrt{n_{xx}^2 - n_{eff}^2}\Big|_{\partial\Omega}$ for TM. At this point, it is clear that the proper boundary conditions is related to the correct choice of the sign of the square root within $k_r$ at the computational boundaries, and using this Sommerfeld-like boundary conditions we can model the confinement of light within the lower refractive index layer(s) of the structure. Using chain rule and eq. (7), we can finally get $\partial_x\varphi = \hat{r} \bullet \hat{x}\ \partial_r\varphi = -ik_r\,(\hat{r} \bullet \hat{x})\ \varphi$ which is required to evaluate the boundary terms. Here, the hat ($\hat{}$) symbol denotes the unit vector. It should be noted that since $n_{eff}^2$ as the matrix eigenvalue also resides within the boundary terms, the matrix eigenvalue equation becomes non-linear. In this work, we solve this using a simple iteration scheme, which enable us to use a linear matrix eigenvalue solver within each iteration step.

## 3. RESULTS AND DISCUSSIONS

Here, we take several types of structures that comprise of lower refractive index of core layer(s) than its substrate and/or cladding, and use the mathematical tool described in the previous section to calculate their leaky modes. The results

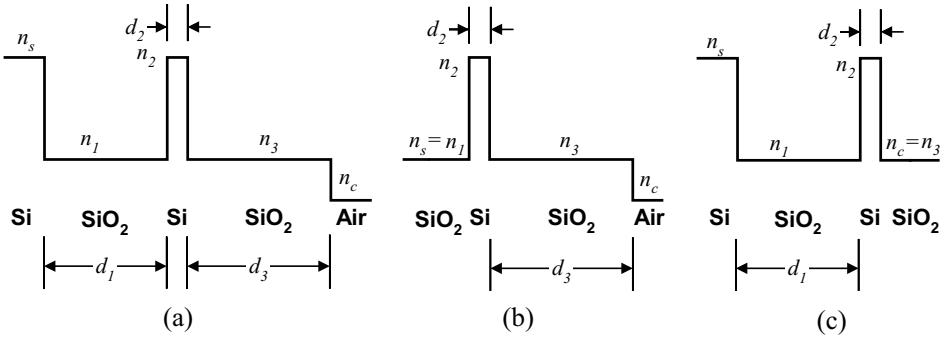


Figure 1: (a). The ARROW structure and its simplified structure (b). by setting $n_s$=$n_1$ and (c). $n_c$=$n_3$.

will be interpreted and discussed. The structures range from ARROW, step- and graded-index waveguides made on high-index substrate, planar Bragg and hollow waveguides.

### 3.1. Arrow Structure

As the first example, we take an ARROW structure, which is the same structure as the one calculated by Kubica *et al.* [4] and Liu *et al.* [7]. The structure is as shown in Fig. 1a with $n_s$=3.5, $n_1$=1.45, $n_2$=3.5, $n_3$=1.45, $n_c$=1, $d_1$=2.0985$\mu$m, $d_2$=0.1019$\mu$m, and $d_3$=4$\mu$m. The computation was carried out for light vacuum wavelength of 1.3$\mu$m. The calculated mode indices, dispersion and confinement loss curves as function of both $d_1$ and $d_3$ are given elsewhere [11] and agree well with the results of others. Fig. 2 and 3 show the mode profile of few leaky modes of the corresponding structure. It is obvious from the mode profiles that the modes are quasi-confined within the low refractive index core layer(s) of the structure. The mode profiles also show the wave-like profile in the high-index substrate, which indicate the leakage of power toward the substrate, and an evanescent decay profile in the low-index cladding. As the leakage loss getting higher, e.g. for the TM-polarized modes, the wave-like profiles become more noticeable. As has been shown in our previous paper [11], the dispersion curves of this structure comprise of parts with dispersive and non-dispersive properties, with the dispersive part related to modes that are quasi-confined mainly in the $SiO_2$ layer corresponding to the horizontal axis of the dispersion curves and the non-dispersive part related to modes quasi-confined within the other $SiO_2$ layer. Hence, the unusual dispersion curves of this structure can be attributed to the anti-crossing between the core and the second-cladding (i.e. the cladding with thickness $d_1$) resonance modes. This argument has been shown by superimposing the dispersion curves with those of simplified structure i.e. the one with $n_s$=$n_1$ (Fig. 1b) and $n_c$=$n_3$ (Fig. 1c) in our

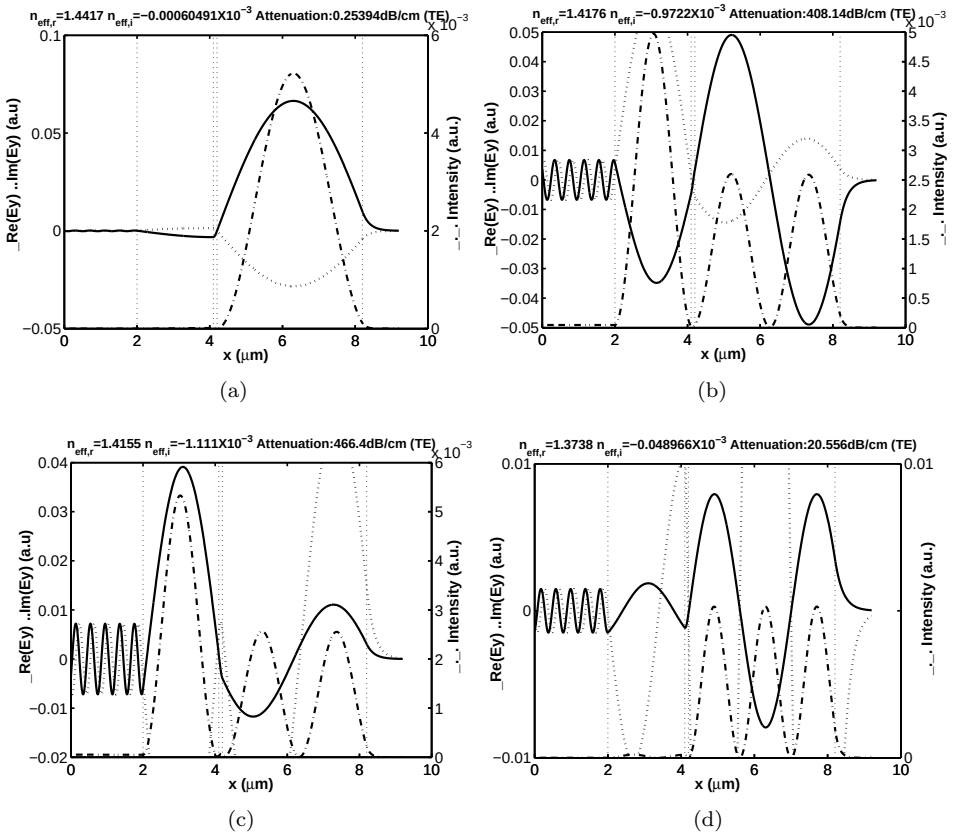


Figure 2: Mode profiles of (a). $\mathrm{TE}_{0,L}$ (b). $\mathrm{TE}_{1,L}$ (c). $\mathrm{TE}_{2,L}$ and (d). $\mathrm{TE}_{3,L}$ of the ARROW structure.

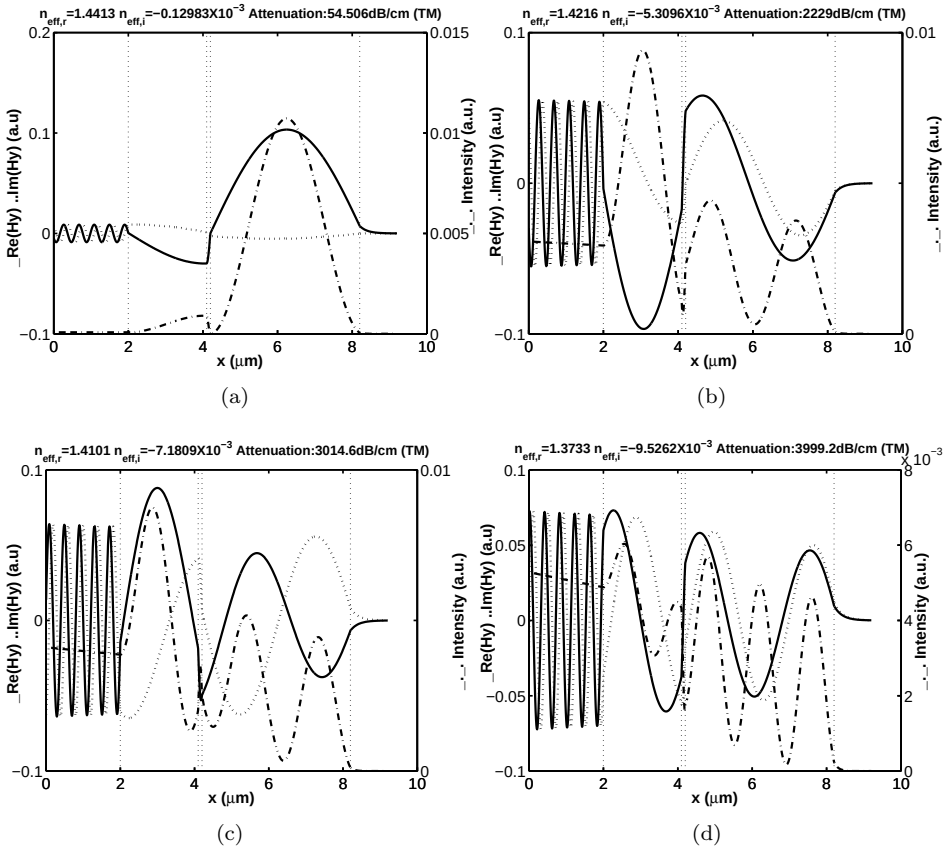


Figure 3: Mode profiles of (a). $TM_{0,L}$ (b). $TM_{1,L}$ (c). $TM_{2,L}$ and (d). $TM_{3,L}$ of the ARROW structure.

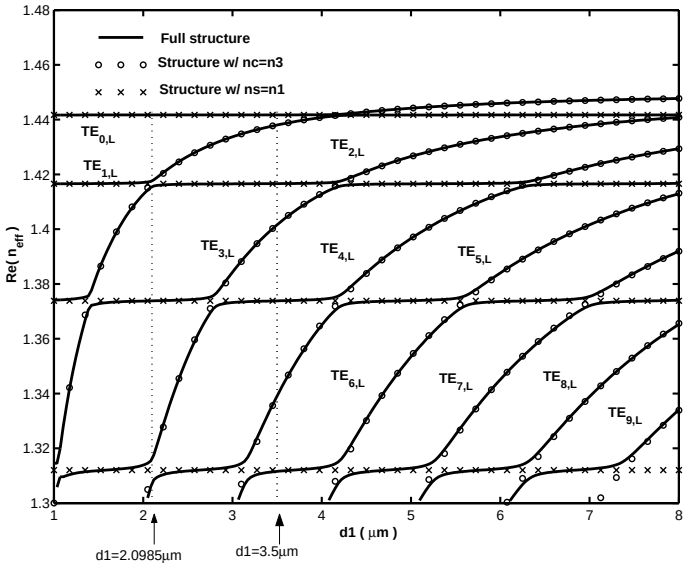


Figure 4: Dispersion curves by changing $d_1$. At $d_1$=3.5 $\mu$m we will have mode $\mathrm{TE}_{0,L}$ to be non-dispersive, $\mathrm{TE}_{1,L}$ to be dispersive, $\mathrm{TE}_{2,L}$ to be non-dispersive, etc.

previous paper, which for the sake of clarity is shown again in Fig. 4. In this figure the mode labeling is only shown for the full structure. To further emphasize the relation between mode confinement and the dispersion curves properties, we herewith show the mode profiles for $d_1$=3.5 $\mu$m for the full and the simplified structures. For this thickness of $d_1$ we will have modes $\mathrm{TE}_{0,L}$ to be non-dispersive, $\mathrm{TE}_{1,L}$ dispersive, $\mathrm{TE}_{2,L}$ non-dispersive, etc. with respect to $d_1$ as shown by Fig. 4. The mode profiles depicted in Fig. 5 clearly show the similarity of mode confinement between the modes of the full structure with the associated simplified structures. This relation explains the number of peak(s) of the mode profiles within the quasi-confined layer that is somehow different from the mode profiles of ordinary waveguides. This also explains why the mode profiles of Fig 2b, 2c, 3b, 3c, and 3d are quasi-confined within both $SiO_2$ layers, as the modes are located around the transition between the dispersive and the non-dispersive parts of the curves; or in other word, around the anti-crossings between the core and the second-cladding resonance modes, where the coupling between these two modes are relatively high. Fig. 5 also shows that the modes that are quasi-confined within the $SiO_2$ layer nearest to the high-index substrate will suffer from higher loss as it can easier leak out toward the substrate than the one quasi-confined within the other $SiO_2$ layer. If we can by some manner switch a mode from the dispersive to the non-dispersive region or vice versa; we would expect the mode quasi-confinement to switch from one to the other $SiO_2$

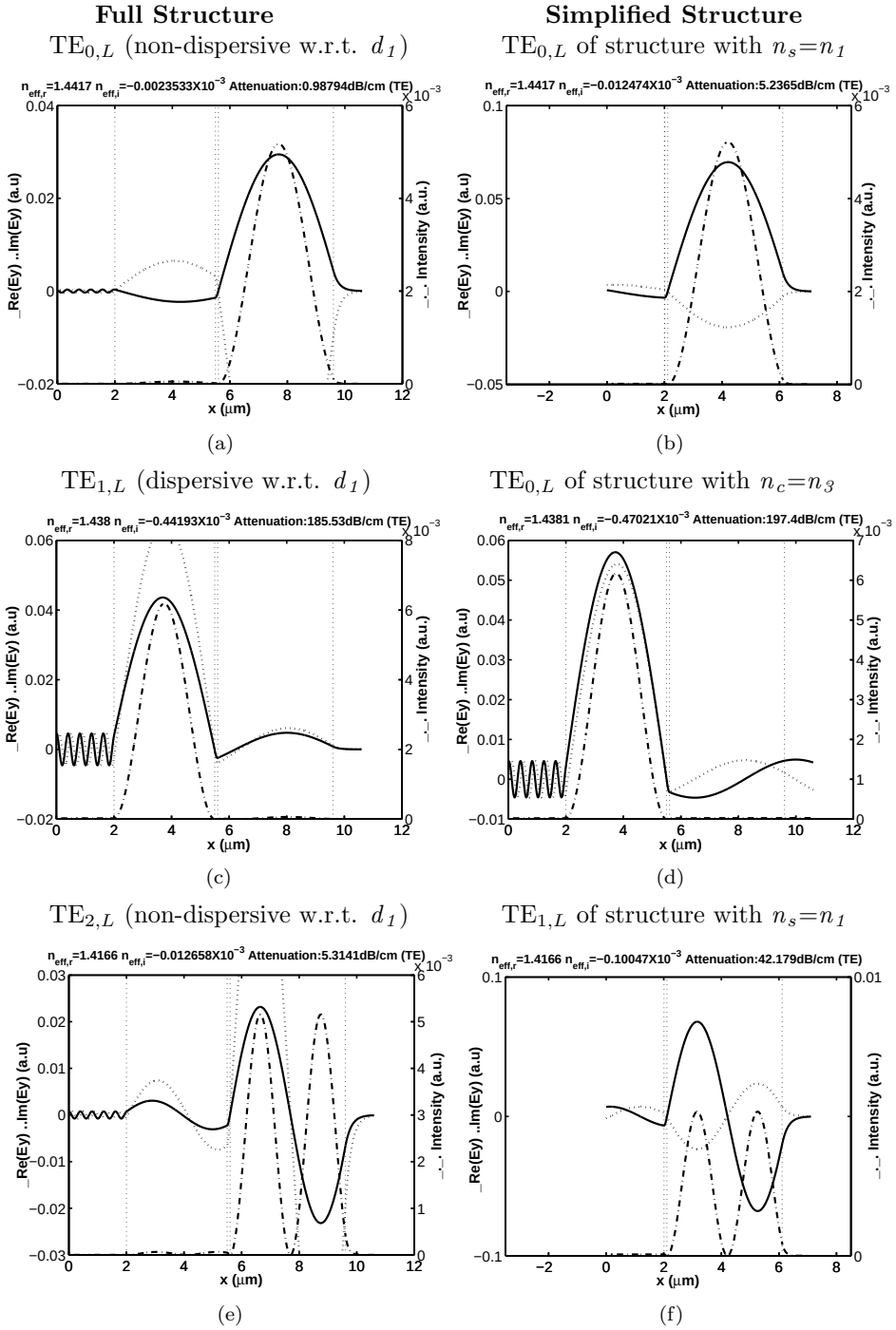


Figure 5: Mode profiles of the full structure (left column) and the corresponding mode profiles of the simplified structures (right column) for $d_1$=3.5$\mu$m.

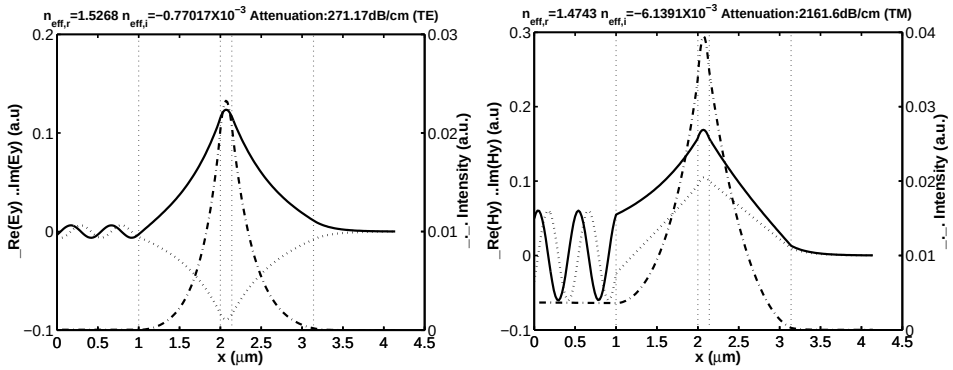


(a) (b)

Figure 6: Mode profile, mode indices, and leakage loss of the step-index silicon nitride planar waveguide: (a). the TE and (b). the TM-polarized modes.

layer, or from high leakage loss to low leakage loss properties, or vice versa; which can be utilized for switching or sensing applications.

### 3.2. Step-Index Leaky Waveguide

For the step-index leaky waveguide, we take a planar waveguide made of $Si_3N_4$ core on a thermally oxidized Si wafer and covered with PE-CVD grown $SiO_2$ cladding with air as the outermost cladding. The light is expected to be quasi-confined within the $Si_3N_4$ layer, with the thermally oxidized $SiO_2$ plays the role as a buffer layer to reduce the leakage of the power toward the high-index Si substrate. The refractive indices of the Si, $SiO_2$ by oxidation, $Si_3N_4$, $SiO_2$ by PE-CVD, and air cladding are 3.476, 1.45, 1.98, 1.464, and 1, respectively at light wavelength of 1.55 $\mu$m. The thickness of the buffer layer, the $Si_3N_4$ core, and the $SiO_2$ cladding are 1 $\mu$m, 0.14 $\mu$m, and 1 $\mu$m, respectively. The calculated mode indices and mode profiles are shown in Fig. 6. It shows that the light is quasi-confined within the $Si_3N_4$ layer, which has lower refractive index than the Si substrate. For this weakly guiding and thin-buffer configuration, the leakage loss is rather high.

Figure 7 shows the mode and intensity profiles if we put the lower computational boundary at 20 $\mu$m and 100 $\mu$m depth inside the substrate. It clearly shows that the mode and intensity profile grow as we move our inspection point further into the substrate. As a consequence, the mode can not be normalized and hence some people regard this leaky mode as non-physical [1]. Here, we would like to interpret this field and intensity growing up from the mode solving point of view.

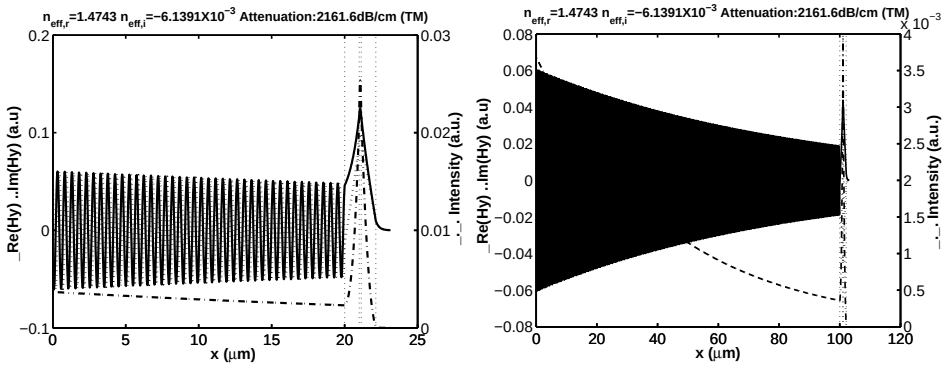


(a) (b)

Figure 7: Mode profile of $TM_{0,L}$ for the lower computational boundary located at (a). 20 $\mu$m and (b). 100 $\mu$m depth inside the substrate.

As mode solving is looking for steady state solution of a waveguiding structure, we should aware that the solutions correspond to a structure that longitudinally extends from $z$ = -$\infty$. Hence, we can interpret the field growing up as contributions from leakage of fields starting from $z$ = -$\infty$. Alternatively, we might interpret this field growing up as an indication of the presence of leakage loss. If we launch a field into the structure, for short distance we will see that the field will be confined within the core. But as it travels through the structure, the field profile will slowly evolved into the profile where the field in the high index substrate/cladding is much larger than in the core, which means that there is leakage of energy toward the high-index substrate/cladding. Hence, the field is not fully confined, but only quasi-confined within the core, which is effective only for short distance. If we have thick enough buffer layer, the leakage loss will be small enough to enable utilization of the quasi-guiding of light for functional integrated optical circuits as has been demonstrated by de Ridder *et al.* [8].

### 3.3. Leaky Graded-Index Waveguide

This sample is a leaky graded-index waveguide made of anisotropic materials, i.e. graded-index $SiO_xN_y$ waveguide grown on a high index Si substrate, where the index gradient can be generated by changing the composition of the source gases during the deposition process through a computer-controlled mechanism [5]. The refractive index profile of the structure is given in Fig. 8. The refractive index of the silicon substrate is $n_s$=3.476, while the refractive index profile of the anisotropic

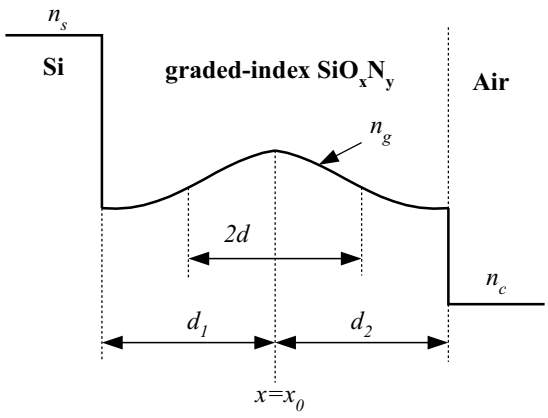


Figure 8: Refractive index profile of a Gaussian $SiO_xN_y$ leaky structure.

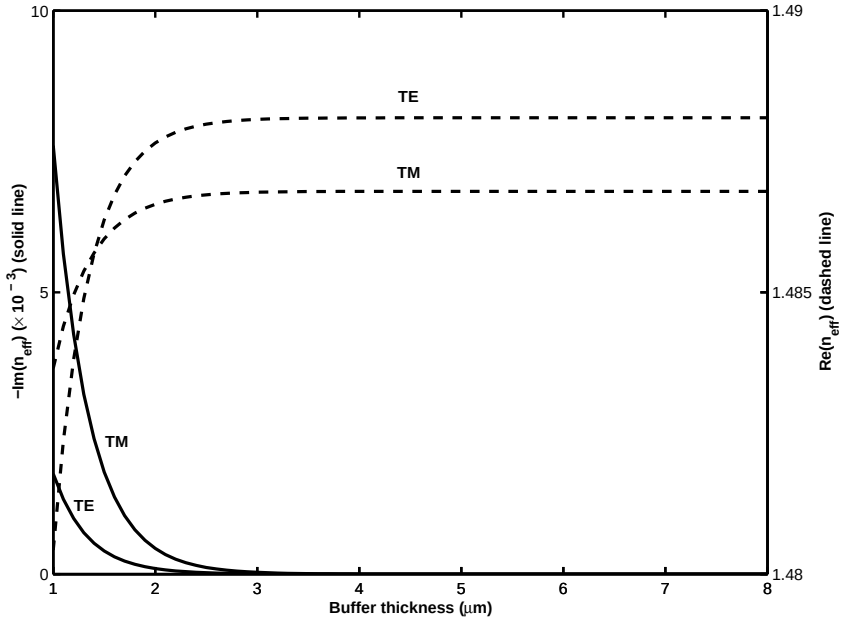


Figure 9: Dependence of the real and the imaginary part of the mode effective indices on the buffer thickness ($d_1$) for the leaky graded-index anisotropic waveguide.

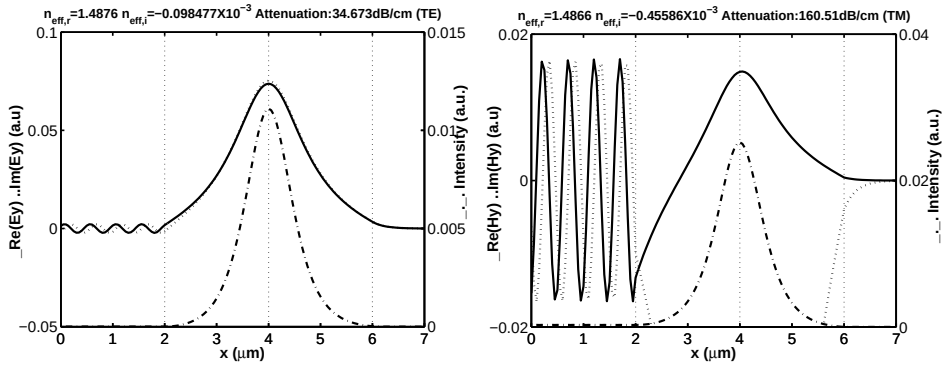


(a) (b)

Figure 10: The mode and intensity profiles of the leaky graded-index anisotropic waveguide for $d_1$=2$\mu$m. (a). TE and (b). TM polarization.

graded-index $SiO_xN_y$ follows

$$n_g = n_{lo} + \Delta \exp\left[-\left(x - x_0\right)^2 / d^2\right]$$

with $n_{lo,xx}$=$n_{lo,yy}$=$n_{lo,zz}$=1.45, $\Delta_{xx}$=0.1, $\Delta_{yy}$=$\Delta_{zz}$=0.098, $d$ =0.5$\mu$m, and the vacuum wavelength of $\lambda$=1.55$\mu$m. The cladding of the structure is air with $n_c$ =1. The position of the peak of the $SiO_xN_y$ index profile from the waveguide-air interface is $d_2$ =2$\mu$m, while $d_1$ being varied from 1 to 8 $\mu$m. The dependence of the real and imaginary part of the effective indices on the graded-index buffer thickness ($d_1$) which will effect the mode phase velocity and leakage loss, respectively; are shown in Fig. 9, while the mode profiles for $d_1$=2$\mu$m are shown in Fig. 10. As shown by Fig. 9, the real part of effective indices approach the effective indices of the lossless structure (without high-index substrate) from below while the imaginary part of the effective index getting smaller (means smaller leakage) as we increase the thickness of the buffer layer. It is interesting to note here, that the stronger the effect of the high-index Si substrate (induced by smaller $d_1$), the lower the real part of the effective indices. This contra-intuitive trend comes from the fact that the refractive index of the Si substrate is located beyond a threshold value called as the zero-crossing point for TE or between two zero-crossing points for TM, as can be shown by using a perturbation analysis [12]. Fig. 9 also shows that at very thin buffer configuration, the real part of the effective index of the TM-polarized mode can be larger than the one of the TE while for thick buffer it will be smaller than TE as in ordinary waveguides.

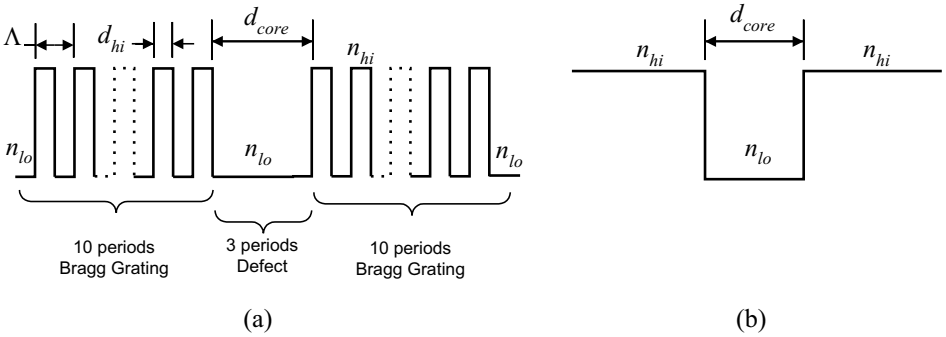


Figure 11: The refractive index profile of (a). the Bragg and (b). the hollow waveguide.

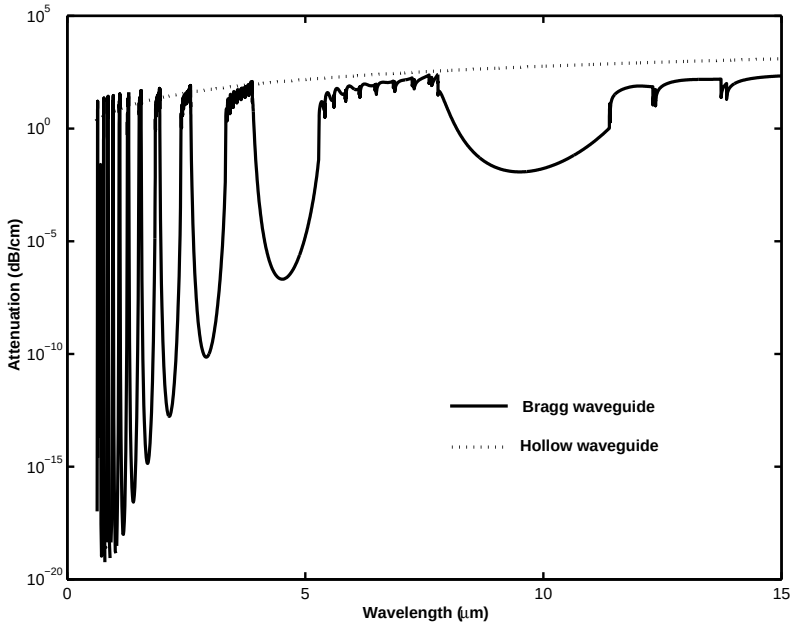


Figure 12: Attenuation due to leakage loss of the Bragg and the hollow waveguide as function of wavelength for $\mathrm{TE}_{0,L}$ mode.

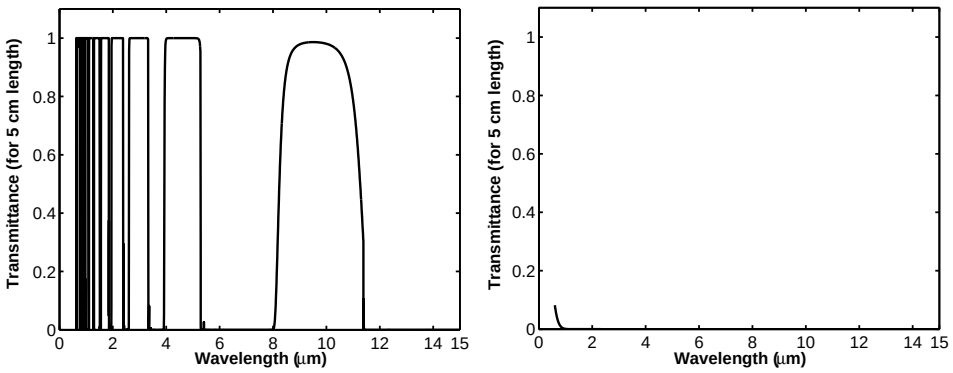


(a) (b)

Figure 13: The transmittance of (a). the Bragg and (b). the hollow waveguide for length of 5 cm for $TE_{0,L}$ mode.

### 3.4. Planar Bragg and Hollow Waveguide

Finally, we investigate planar Bragg and hollow waveguides with refractive index profile as depicted in Fig. 11. We pick up a Bragg waveguide with similar parameters as the one analyzed by Litchinitser *et al.* [6] and take a hollow waveguide of comparable size. The Bragg waveguide quasi-guides light by the help of Bragg reflection as proposed by Yeh and Yariv [13]. The period of the 10-period Bragg grating that acts as the cladding at each side of the Bragg waveguide is $\Lambda$=5$\mu$m with refractive index of $n_{hi}$=1.8 and $n_{lo}$=1.4 and thickness of high index layer of $d_{hi}$=3.437$\mu$m. With a defect due to missing of high index region in 3 periods, the width of the low index core of the waveguide is $d_{core}$=4$\Lambda$-$d_{hi}$. The associated hollow waveguide has the same width of the low index core with the same homogeneous high index cladding at both sides.

By neglecting the material chromatic dispersion, the leakage loss and the associated transmittance curves calculated from the imaginary part of the mode indices for the fundamental TE mode of both waveguide for wavelength changes from 0.6 to 15 $\mu$m are given in Fig. 12 and 13. The mode profiles of the two-first TE and TM modes of both structures at wavelength of 1$\mu$m are given in Fig. 14 and 15. Fig. 12 shows that the leakage of power in the hollow waveguide steadily increases by the increase of the wavelength while for the Bragg waveguide at certain wavelength regions where the modal transverse wavenumber corresponds to or around the Bragg wavenumber of the grating, the grating helps to decrease the leakage. Fig. 13a is qualitatively similar to the results of BPM simulation given by Litchinitser *et al.* [6]. Note that at some parts of the curve, Litchinitser *et al.*

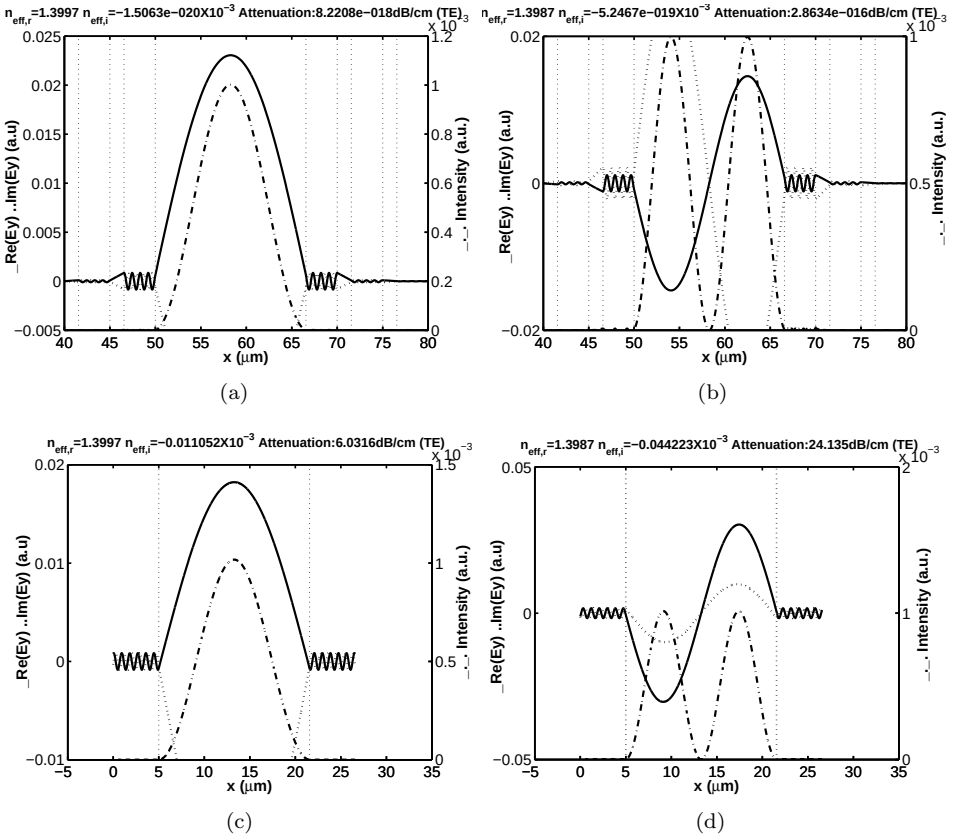


Figure 14: The mode profiles of (a). $\mathrm{TE}_{0,L}$, (b). $\mathrm{TE}_{1,L}$ of the Bragg waveguide and (c). $\mathrm{TE}_{0,L}$ and (d). $\mathrm{TE}_{1,L}$ of the hollow waveguide for $\lambda$=1$\mu$m. Note that to ease the comparison, the plotting windows do not coincide with the computational domain size.

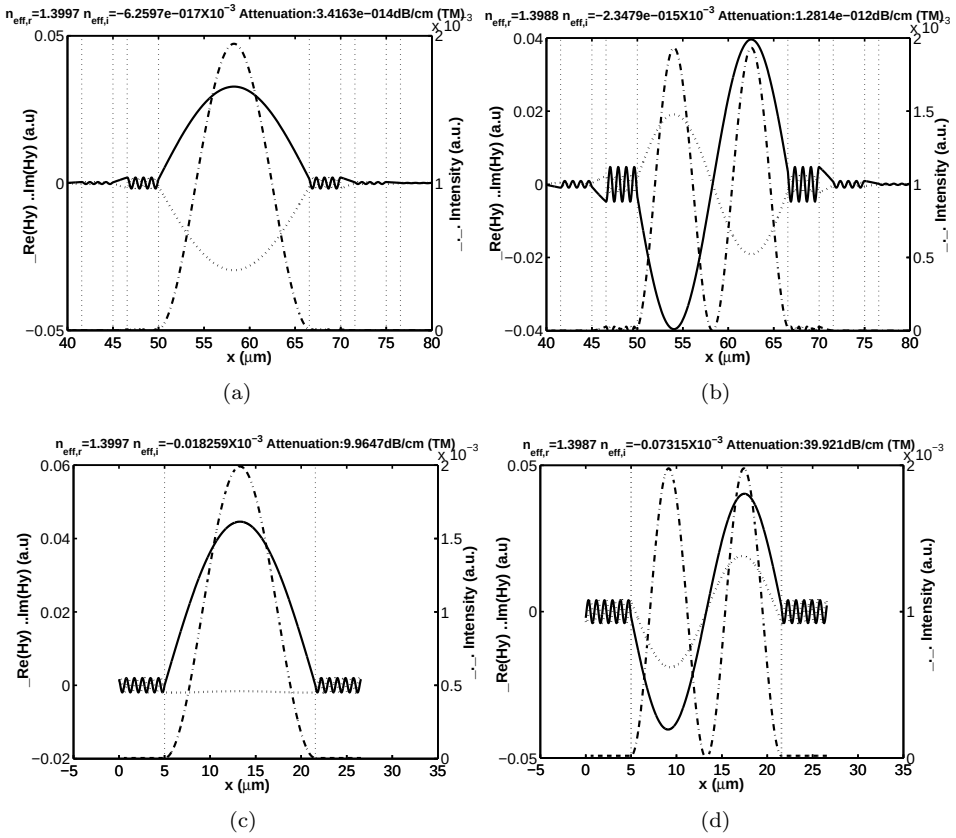


Figure 15: The mode profiles of (a). $\mathrm{TM}_{0,L}$, (b). $\mathrm{TM}_{1,L}$ of the Bragg waveguide and (c). $\mathrm{TM}_{0,L}$ and (d). $\mathrm{TM}_{1,L}$ of the hollow waveguide for $\lambda$=1$\mu$m. Note that to ease the comparison, the plotting windows do not coincide with the computational domain size.

got lower transmittance, which we believe comes from the low overlap between the Gaussian excitation field used by them with the mode profile of the waveguide, especially to the wave-like tail of the mode profile. Fig. 14 and 15 show similar mode profiles and real part of mode effective indices of the two structures, but with much lower leakage loss of the Bragg waveguide. As the Bragg wavenumber of the grating is sensitive to the refractive index changes of the material, the Bragg waveguide can be applied as a refractive index sensor of e.g. liquid or gases that can be used to form the low index part of the structure.

## 4. CONCLUSIONS

It is shown that using mathematical tools with proper boundary conditions, we can model the quasi-guiding of light within the core(s) with lower refractive index than the surrounding(s) (substrate and/or cladding). Galerkin FEM furnished with Sommerfeld-like boundary conditions has been used for this purpose. The method is demonstrated using some samples including ARROW, leaky graded-index anisotropic waveguide, Bragg and hollow waveguide; where the quasi-confinement of light within the low index core was illustrated and interpreted through the mode profiles.

**Acknowledgement.** The support of STW Technology Foundation to the Ph.D. work of H.P. Uranus through project TWI.4813 is acknowledged.

## REFERENCES

1. P. Bienstman and R. Baets, "Advanced boundary conditions for eigenmode expansion models", *Opt. Quantum Elect.* **34** (2002), 523-540.
2. W. Huang, R.M. Shubair, A. Nathan, and Y.L. Chow, "The modal characteristics of ARROW structures", *J. Lightwave Technol.* **10** (1992), 1015-1022.
3. W.P. Huang, C.L. Xu, W. Lui, and K. Yokoyama, "The perfectly matched layer boundary condition for modal analysis of optical waveguides: leaky mode calculations", *Photonics Technol. Lett.* **8** (1996), 652-654.
4. J. Kubica, D.Uttamchandani, and B. Culshaw, "Modal propagation within ARROW waveguides", *Opt. Commun.* **78** (1990), 133-136.
5. S. Lim, S. Shih, and J.F. Wager, "Design and fabrication of a double bandstop rugate filter grown by plasma-enhanced chemical vapor deposition", *Thin Solid Films* **277** (1996), 144-146.
6. N.M. Litchinitser, A.K. Abeeluck, C. Headly, and B.J. Eggleton, "Antiresonant reflecting photonic crystal optical waveguides", *Opt. Lett.* **27** (2002), 1592-1594.
7. B. Liu, A. Shakouri, and J.E. Bowers, "Characteristic equations for different ARROW structures", *Opt. Quantum Elect.* **31** (1999), 1267-1276.

8. R.M. de Ridder, K. Wörhoff, A. Driessen, P.V. Lambeck, and H. Albers, "Silicon oxynitride planar waveguiding structures for application in optical communication", *J. Sel. Topics in Quantum Elect.* **4** (1998), 930-937.
9. Y. Tsuji and M. Koshiba, "Guided-mode and leaky-mode analysis by imaginary distance beam propagation method based on finite element scheme", *J. Lightwave Technol.* **18** (2000), 618-623.
10. R. Ulrich and W. Prettl, "Planar leaky light-guides and couplers", *Applied Phys.* **1** (1973), 55-68.
11. H.P. Uranus, H.J.W.M. Hoekstra, and E. van Groesen, "Simple high-order Galerkin finite element scheme for the investigation of both guided and leaky modes in anisotropic planar waveguides", *Opt. and Quantum Elect.* **36** (2004), 239-257.
12. H.P. Uranus, H.J.W.M. Hoekstra, and E. van Groesen, "Finite element and perturbative study of buffered leaky planar waveguides", to appear in *Opt. Commun.*
13. P. Yeh and A. Yariv, "Bragg reflection waveguides", *Opt. Commun.* **19** (1976), 427-430.

H.P. Uranus: Integrated Optical MicroSystems Group and Applied Analysis and Mathematical Physics Group, MESA$^+$ Research Institute, University of Twente, P.O. Box 217, 7500 AE Enschede, The Netherlands.
e-mail: h.p.uranus@ewi.utwente.nl.

H.J.W.M. Hoekstra: Integrated Optical MicroSystems Group, MESA$^+$ Research Institute, University of Twente, P.O. Box 217, 7500 AE Enschede, The Netherlands.
e-mail: h.j.w.m.hoekstra@ewi.utwente.nl.

E. van Groesen: Applied Analysis and Mathematical Physics Group, MESA$^+$ Research Institute, University of Twente, P.O. Box 217, 7500 AE Enschede, The Netherlands.
e-mail: groesen@math.utwente.nl.